Inorganic Chemistry

Article

pubs.acs.org/IC

Magnetic Interactions through Fluoride: Magnetic and Spectroscopic Characterization of Discrete, Linearly Bridged $[Mn^{III}_2(\mu\text{-}F)F_4(Me_3tacn)_2](PF_6)$

Kasper S. Pedersen,[†] Marc Sigrist,[†,‡] Høgni Weihe,[†] Andrew D. Bond,[§] Christian Aa. Thuesen,[†] Kim P. Simonsen,[⊥] Torben Birk,[†] Hannu Mutka,[‡] Anne-Laure Barra,[∥] and Jesper Bendix*[,†]

[†]Department of Chemistry, University of Copenhagen, Universitetsparken 5, DK-2100 Copenhagen, Denmark

[‡]Institut Laue-Langevin, F-38042 Grenoble Cedex 9, France

[§]Department of Physics and Chemistry, University of Southern Denmark, Campusvej 55, 5230 Odense M, Denmark

[⊥]School of Conservation, The Royal Academy of Fine Arts Schools of Architecture, Design and Conservation, Esplanaden 34, DK-1263 Copenhagen, Denmark

[∥]Laboratoire National des Champs Magnétiques Intenses, CNRS, BP 166, F-38042 Grenoble Cedex 9, France

Supporting Information

ABSTRACT: The nature of the magnetic interaction through fluoride in a simple, dinuclear manganese(III) complex (**1**), bridged by a single fluoride ion in a perfectly linear fashion, is established by experiment and density functional theory. The magnitude of the antiferromagnetic exchange interaction and the manganese(III) zero-field-splitting parameters are unambiguously determined by inelastic neutron scattering to yield J = 33.0(2) cm^{-1} ($\hat{H} = J\hat{S}_1\cdot\hat{S}_2$ Hamiltonian definition) and single-ion D = −4.0(1) cm^{-1}. Additionally, high-field, high-frequency electron paramagnetic resonance and magnetic measurements support the parameter values and resolve $|E| \approx 0.04$ cm^{-1}. The exchange coupling constant (J) is 1 order of magnitude smaller than that found in comparable systems with linear oxide bridging but comparable to typical magnitudes through cyanide, thus underlining the potential of fluoride complexes as promising building blocks for novel magnetic systems.

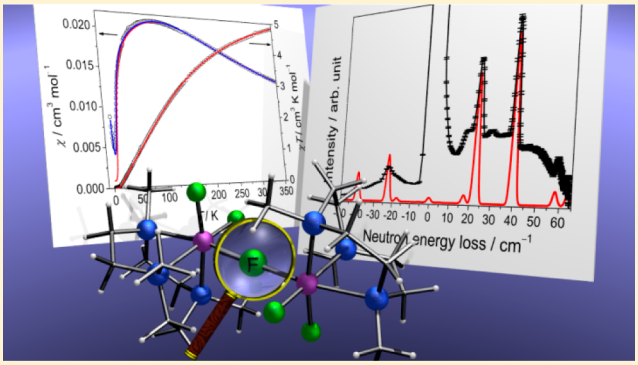

INTRODUCTION

Polynuclear manganese(III) complexes encompassing oxide or hydroxide bridging ligands are very well-established in the literature because of a massive interest in, e.g., record-large spin ground states,[1] slow relaxation of magnetization in isolated molecules (single-molecule magnets),[2] and higher-dimensionality structures such as one-dimensional (single-chain magnets).[3] Remarkably less studied are polynuclear complexes encompassing bridging fluoride ligands. The oxide-isoelectronic fluoride ion is a promising choice as the bridging ligand in paramagnetic dinuclear or polynuclear transition-metal and lanthanide complex chemistry because of the spectroscopic innocence, the complete absence of redox activity, and an apparent, intrinsic preference for linear bridging.[4] In addition, owing to the relatively low basicity of fluoride, several mononuclear fluoride complexes have the possibility of directly serving in a modular approach, as structure-directing building blocks toward higher-nuclearity structures.[5] This is, in general, an unlikely synthetic pathway for hydroxide- or oxide-based complexes, where accessibility to discrete precursors suitable as modules is limited by a tendency toward solvolysis and oligomerization. Fluoride as a bridging ligand has been intensively employed by Winpenny, Timco, and co-workers in homo- and heterometallic wheels[6] or chain fragments ("horseshoes").[7] For these systems, $CrF_3\cdot 4H_2O$ has been employed as a simple starting material. For manganese, analogous use of the simplest manganese(III) source, MnF_3, to build polynuclear complexes was first reported by Brechin, Collison, and co-workers.[8] Also, a few partly fluoride-bridged, polynuclear manganese(III) complexes have been obtained by fluoride abstraction from BF_4^- [9] or Et_2NSF_3.[10] In all those systems, the bridging fluoride ligands are supported by other bridging ligands. In extended structures, fluoride is more commonly found without bridging coligands, and the magnetic properties of such systems have attracted some attention.[11] In addition comes a series of one-dimensional chains with general formulas $AMn^{III}F_4\cdot H_2O$ and $A_2Mn^{III}F_5\cdot xH_2O$ incorporating *trans*-$[Mn^{III}F_4F_{2/2}]^{2-}$ and eventually *trans*-$[Mn^{III}F_4(H_2O)_2]^-$ as bridging units.[12] The magnetic properties for such systems are

Received: January 8, 2014
Published: March 7, 2014

   dx.doi.org/10.1021/ic500049w | *Inorg. Chem.* 2014, 53, 5013−5019

significantly more complex compared to other 3d polymers because of the strong magnetic anisotropy of manganese(III) imposed by the Jahn−Teller (JT) effect. Recently, we reported on a simple manganese(III) chain with unsupported fluoride bridges obtained by the direct reaction of MnF_3 with H_2salen.[13] Now we present a discrete, dinuclear analogue employing *N*,*N*′,*N*″-trimethyl-1,4,7-triazacyclononane (Me_3tacn) as a capping ligand to prevent polymerization. The reaction of $MnF_3{\cdot}3H_2O$ with Me_3tacn and NH_4PF_6 in a methanolic solution thus yields dinuclear $[Mn^{III}_2(\mu\text{-}F)F_4(Me_3tacn)_2](PF_6)$ (**1**) with a crystallographically linear fluoride bridge. Because **1** constitutes the first molecular manganese(III) entity with a single unsupported fluoride bridge, detailed information about the nature and magnitude of the interactions can be obtained with much greater confidence than was possible for the extended or oligomeric systems because next-nearest and more distant interactions are absent. Here we present a multitechnique study involving magnetic measurements, high-field/frequency electron paramagnetic resonance (HF-EPR), and inelastic neutron scattering (INS) spectroscopy to characterize in detail the magnetic interactions in **1**. The use of INS allows for a rigorous direct determination of not only magnetic Mn^{III}−Mn^{III} exchange interaction through the bridging fluoride but also single-ion anisotropies.

EXPERIMENTAL SECTION

Synthesis. Me_3tacn and $MnF_3{\cdot}3H_2O$ were synthesized as described in the literature.[14,15] NH_4PF_6 and solvents were obtained from commercial sources and used as received. Me_3tacn (136 mg, 0.794 mmol) and $MnF_3{\cdot}3H_2O$ (130 mg, 0.783 mmol) were dissolved in methanol (2.5 mL). The solution turned deep-red-orange within minutes and was stirred at room temperature for 10 h. The addition of a solution of NH_4PF_6 (500 mg, 3.07 mmol) in methanol (2 mL) resulted in the immediate precipitation of bright-orange crystals. Slow evaporation of the solvent to a volume of ∼3 mL and subsequent filtration by suction gave **1** in 59% (163 mg) yield. The crude **1** was recrystallized from boiling methanol (25 mL), yielding 112 mg of product. Elem anal. Calcd for $C_{18}H_{42}F_{11}Mn_2N_6P$: C, 31.22; H, 6.11; N, 12.14. Found: C, 30.74; H, 6.02; N, 11.94.

Crystallography. Single-crystal X-ray diffraction data were collected at 122 K on a Bruker Nonius X8 APEX-II CCD diffractometer employing Mo Kα radiation (λ = 0.71073 Å). The structures were solved using direct methods (*SHELXS97*) and refined using the *SHELXL97* software package.[16] All non-hydrogen atoms were refined anisotropically, whereas hydrogen atoms were fixed as riding their parent atom in a fixed geometry. CCDC 986307 contains the supplementary crystallographic data for this paper. These data can be obtained free of charge from The Cambridge Crystallographic Data Centre via www.ccdc.cam.ac.uk/data_request/cif. Table 1 summarizes the crystallographic data and refinement parameters.

Magnetic Measurements. The magnetic characterization was performed on a Quantum-Design MPMS-XL SQUID magnetometer equipped with a 5 T direct-current (dc) magnet. The magnetization was measured in H_{dc} = 1000 Oe from 2 to 350 K on polycrystalline samples in polycarbonate capsules. The modeling and fitting of magnetic data were performed with *MagProp*,[17] which is a part of the *DAVE* program suite.[18] The susceptibility (χ) was calculated as $\chi = M/H$ and corrected for diamagnetic contributions from the sample (by means of Pascal constants) and capsule.

INS Spectroscopy. INS spectra were obtained by the direct geometry, time-of-flight spectrometer IN5 at the Institut Laue-Langevin, Grenoble, France. Approximately 0.5 g of a nondeuterated polycrystalline sample was loaded into a 10-mm-diameter double-wall hollow aluminum cylinder. A standard ILL Orange cryostat was employed. The data were reduced and analyzed using the *LAMP* program package.[19] The INS spectra were calculated using a home-written program, as previously described.[17]

Table 1. Crystallographic Data and Refinement Parameters

formula	$C_{18}H_{42}F_5Mn_2N_6F_6P$
M_r/g mol^{-1}	692.42
color, shape	red, prism
cryst size/mm	0.20 × 0.10 × 0.05
cryst syst	triclinic
space group	$P\bar{1}$
T/K	120(2)
a/Å	7.3362(5)
b/Å	7.4467(6)
c/Å	13.8751(10)
α/deg	75.658 (3)
β/deg	81.412 (3)
γ/deg	72.302 (3)
V/Å^3	697.37 (9)
Z	1
ρ_{calc}/g cm^{-3}	1.649
F_{000}	356
μ(Mo Kα)/mm^{-1}	1.06
θ range/deg	3.5−25.1
indep refIns	2447
param/restraints	206/12
refIns [$I > 2\sigma(I)$]	2257
GOF	1.05
R1[a] [$I > 2.00\sigma(I)$]	0.050
R1[a] (all data)	0.055
wR2[b] (all data)	0.114
max/min $\Delta\rho$/e Å^{-3}	0.93/−0.76

[a] $R1 = \sum||F_o| - |F_c||/\sum|F_o|$. [b] $wR2 = [\sum w(F_o^2 - F_c^2)^2/\sum w(F_o^2)^2]^{1/2}$.

Mass Spectrometry. Mass spectrometry was performed on a Bruker MicroTOF-QII equipped with an electrospray ionization (ESI) source. Samples were prepared by the dissolution of crystalline, washed products in acetonitrile. Direct sample injection was performed using a syringe pump operating at 25−100 μL min^{-1}. With the ion polarity set in the positive mode, the ion transfer and collision cell radio-frequency (RF) voltages were maintained at the following values: funnel 1 at 300 Vpp (peak-to-peak voltage), funnel 2 at 400 Vpp, the hexapole at 400 Vpp, and the collision cell RF at 630 Vpp. An energy of 10.0 eV was applied in the collision cell, and a transfer time of 127 μs with a prepulse storage of 25 μs was used. The drying temperature and end-plate offset of the source were maintained at 150 °C and −500 V, respectively, while the following ionization parameters were manually optimized within the ranges indicated to achieve the highest signal-to-noise ratio and to account for the differences in injection flow rates: capillary voltage, 4500−5500 V; dry gas flow rate, 2.0−8.0 L min^{-1}; nebulizer pressure, 0.1−8.0 bar.

HF-EPR Spectroscopy. EPR data were acquired on powdered samples at the Laboratoire National des Champs Magnétiques Intenses (Grenoble, France). Detailed descriptions of the equipment can be found in ref 20. The spectra were simulated using home-written software.[21]

UV−Vis and Reflectance Spectroscopy. Solution UV−vis spectra were recorded on acetonitrile solutions using a Perkin-Elmer Lambda 2 spectrometer. Solid-state reflectance spectra were recorded using a fiber-optic reflectance spectroscopy setup employing an Ocean Optics USB4000 spectrometer, with a DH-2000-BAL UV−vis−near-IR light source (210−1700 nm; deuterium and halogen lamps). The white standard was Teflon (Mikropack WS-1-SS), and the reflection probe was QR400-7-SR/BX having a core diameter of 400 μm and a wavelength range of 200−1100 nm.

Density Functional Theory (DFT) Calculations. For evaluation of the exchange coupling constants, the broken-symmetry (BS) approach of Noodleman,[22] as implemented in the *ORCA*, version 2.8, suite of programs, was employed.[23] The formalism of Yamaguchi, which employs calculated expectation values $\langle S^2 \rangle$ for both high-spin

dx.doi.org/10.1021/ic500049w | Inorg. Chem. 2014, 53, 5013−5019

and BS states, was used.[24] Calculations related to magnetic interactions were performed using the PBE0 functional. The Ahlrichs-VTZ basis function set was used.[25] Spin densities were visualized using the UCSF *Chimera* program, version 1.5.3.

RESULTS

The reaction of $MnF_3 \cdot 3H_2O$ with Me_3tacn and NH_4PF_6 yields dinuclear **1**. The molecular structure is depicted in Figure 1.

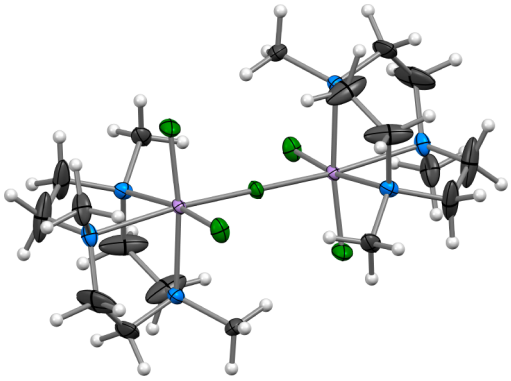

Figure 1. Thermal ellipsoid plot (50% probability level) of **1** as obtained from X-ray crystallography. The PF_6^- counterion is omitted for clarity. Color code: Mn, purple; F, green; N, blue; C, gray; H, white. Selected bond lengths and angles: Mn−$F_{bridging}$ 2.0487(5) Å; Mn−$F_{terminal}$ 1.823(2) Å; Mn−N 2.087(3), 2.096(3), and 2.267(3) Å; Mn−F−Mn 180.0°.

Mononuclear fluoride complexes with tacn-type coligands are reported for Al^{III},[26] Si^{IV},[27] V^{III},[28] Cr^{III},[29] Fe^{III},[30] Ga^{III},[30,31] Ge^{IV},[32] U^{IV} and U^{VI},[33] whereas the reaction of $[Ti^{III}(Me_3tacn)Cl_3]$ with NaF affords fluoride-bridged $[Ti_2(\mu\text{-}F)O_2F_2(Me_3tacn)_2](PF_6)$, which is isomorphous to **1**.[34] In addition, the structure of **1** is similar to recently reported, unusual $[Pd^{III}_2(\mu\text{-}X)X_4(Me_3tacn)_2](PF_6)$ (X = Cl, Br).[35] The bridging fluoride in **1** is located on an inversion center, resulting in a perfectly linear bridging mode. The fact that the elongation (JT) axis coincides with the intermetallic axis is no surprise because the more distant fluoride is more basic and therefore more susceptible to bridging than the closer-bound fluorides.

The magnetization was measured between 1.8 and 350 K in a dc field of 1000 Oe and shown in Figure 2 as χ ($\chi = M/H$) and the χT product. The high-temperature χT value at 350 K of 4.8 cm^3 K mol^{-1} is significantly lower than the value expected for two uncoupled $S = 2$ centers (6.0 cm^3 K mol^{-1} for $g = 2$). This behavior, combined with the observation of a steady decrease in χT upon decreasing temperature, indicates sizable intracomplex antiferromagnetic interactions. The dc susceptibility and spectroscopic experiments were all fitted or simulated by using the spin Hamiltonian:

$$\hat{H} = \mu_B B g \sum_{i=1,2} \hat{S}_i + D \sum_{i=1,2} \left(\hat{S}_{i,z}{}^2 - \frac{1}{3} S(S+1) \right) + E \sum_{i=1,2} (\hat{S}_{i,x}{}^2 - \hat{S}_{i,y}{}^2) + J \hat{S}_1 \cdot \hat{S}_2 \quad (1)$$

where the magnetic interaction between the two manganese(III) ions is represented by an isotropic Heisenberg−Dirac−van Vleck exchange interaction term with coupling constant J. D and E are the usual axial and rhombic zero-field-splitting (ZFS) parameters, respectively. Because of the inversion center localized on the bridging fluoride, the **g** and ZFS tensors of

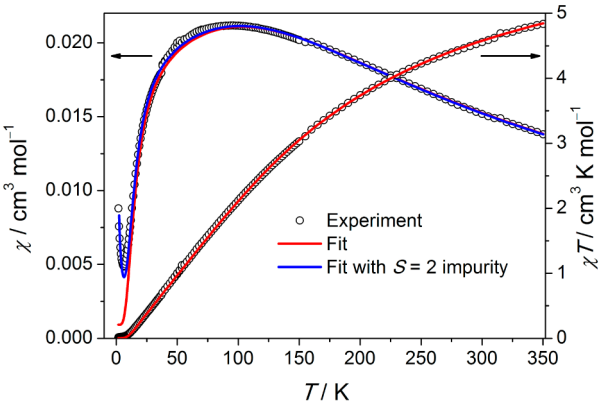

Figure 2. Temperature dependence of the magnetic susceptibility ($\chi = M/H_{dc}$; H_{dc} = 1000 Oe) data for **1** shown as $\chi(T)$ and $\chi(T)T$. The red curve is the best fit. Only J was fitted, whereas the other parameters were fixed to $g = 2.0$, $D = 4.1$ cm^{-1}, and $E = 0$ cm^{-1}. For the blue curve, the fractional concentration (c) of an $S = 2$ Curie spin was fitted while keeping all other parameters frozen, yielding $c \approx 0.6\%$.

Mn1 and Mn2 are identical and coaxial. For the χT product, the leading term is the exchange interaction, whereas single-ion anisotropy is only weakly manifested, even at low temperatures. For that reason, the temperature dependence of χ and χT can be satisfactorily modeled by the inclusion of J only.

However, fixing D to the spectroscopically determined value of −4.0(1) cm^{-1} (vide infra) gives slightly better agreement at the lowest temperatures. The manganese(III) g factors were fixed to 2.0, as suggested by HF-EPR (vide infra). The fitting of dc magnetic data only yields $J = 31.7$ cm^{-1}. The result is shown as solid lines in Figure 2. To gain further confidence in J and insight into the ZFS, INS and HF-EPR were employed. INS has previously shown to be a powerful tool to unravel the low-energy states in polynuclear transition-metal complexes.[36] INS spectra (Figure 3) were acquired with an incident neutron

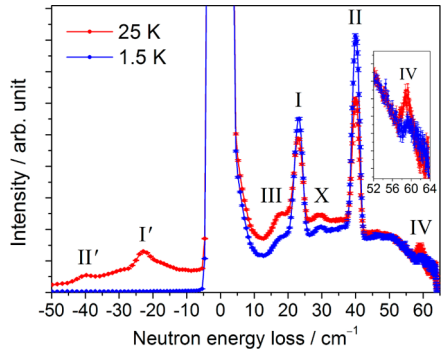

Figure 3. INS spectra acquired at T = 1.5 K (blue) and 25 K (red) with an incident neutron wavelength of λ = 3.0 Å. The data have been summed over the angular range of 6.7−132.5° corresponding to a Q range of 0.24−3.8 $Å^{-1}$ (at the elastic line position). The full width at half-maximum (fwhm) for the elastic lines is 2.9 cm^{-1}, which is close to the fwhm's for I (2.9 cm^{-1}) and II (2.5 cm^{-1}).

wavelength of λ = 3.0 Å at temperatures 1.5 and 25 K. The intensity summation of the detectors over the angular range 6.7−132.5° (Q = 0.24−3.8 $Å^{-1}$) is shown in Figure 3. The Q dependence of the intensity at 1.5 and 25 K is shown in Figures S4 and S5 in the Supporting Information (SI). At low temperature, two prominent energy-loss features are present at neutron energy losses of 23.2(2) cm^{-1} (I) and 40.1(2) cm^{-1}

dx.doi.org/10.1021/ic500049w | Inorg. Chem. 2014, 53, 5013−5019

(II). The features I and II are also visible on the energy-gain side at the higher temperature (25 K) and are given primed labels. Despite the high ^{1}H content of **1**, which commonly gives rise to a high background because of spin-incoherent scattering, the spectra are of high quality and magnetic excitations can be clearly discerned on the basis of the temperature and Q dependences and their line widths.

For features I and II, warming to 25 K leads to a decrease in the intensity, as expected for magnetic ground-state ("cold") excitations. The origin of peak X is unknown, but the temperature independence excludes a magnetic ground-state excitation. Moreover, the intensity scales approximately as Q^2, as expected for a phonon excitation. Upon heating to 25 K, two features, III and IV, emerge. Additionally, for the weak feature IV at ~59.0(7) cm^{-1}, the temperature dependence and narrow fwhm also indicate a "hot" magnetic transition.

From analysis of the magnetic data, the ground state was found to be S = 0 and the transitions (I and II) are attributed to excitations from the S = 0 to 1 state, with the latter being split by the D term (Figures 4 and 5). For D < 0, as is normally

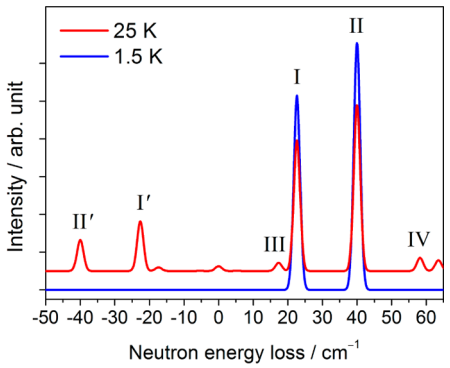

Figure 4. Calculated magnetic part of the INS spectra obtained as described in the main text. The simulated spectra are offset to improve clarity. In addition, the slight energy-transfer dependence of the resolution has not been included in the calculations but included in the uncertainties on the experimental peak positions.

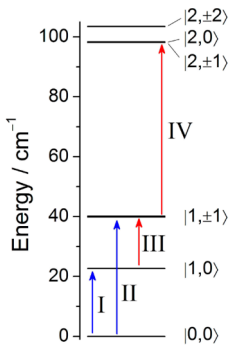

Figure 5. Energy-level diagram derived from analysis of the INS spectra. Blue and red arrows designate "cold" and "hot" excitations, respectively. The ordering of the M_S for S = 2 is as indicated in the figure because of interactions of the |2, 0⟩ state with |0, 0⟩.

encountered in elongated manganese(III) complexes,[37] the qualitative interpretation yields $|S, M_S\rangle$ = |0, 0⟩ to |1, 0⟩ (feature I) and to |1, ±1⟩ (feature II). The "hot" transition III [18.1(2) cm^{-1}] is a magnetic excitation between the two latter states. From the fitting of the INS peak positions (except III), the best-fit parameters were J = 33.0(2) cm^{-1} and an axial single-ion anisotropy parameter of D = −4.0(1) cm^{-1}. The observed and calculated line positions are shown in Table 2.

Table 2. Observed and Fitted INS Peak Positions with J = 33.0(2) cm^{-1} and D = −4.0(1) cm^{-1}

transition	obsd/cm^{-1}	fit/cm^{-1}
I	23.2(2)	23.1
II	40.1(2)	40.0
III	18.1(2)	17.3
IV	59.0(7)	58.9
I′	−23.0(5)	−23.1
I″	−39.7(8)	−40.0

The D value is in good agreement with the values determined for monomeric manganese(III) complexes in similar coordination spheres.[38] Note that no E term was necessary to satisfactorily model the INS data. Reversing the sign of the D parameter results in a poorer agreement of the calculated transition intensities with the experiment, where the intensity of peak I becomes larger than that of peak II.

The HF-EPR spectra (Figures 6 and S6 in the SI) can be well reproduced by simulation employing a slightly larger ZFS

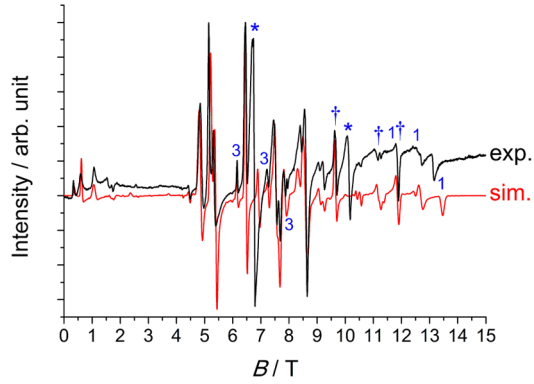

Figure 6. HF-EPR spectra obtained at T = 35 K and ν = 189.9982(2) GHz with a 10% presence of overtone 285 GHz radiation. The three main peaks from the latter frequency are indicated with daggers (†). The transitions indicated by asterisks (*) arise from minor g = 2 impurities. "1" and "3" designate transitions from the S = 1 and 3 multiplets, respectively. Remaining transitions arise from the S = 2 manifold. Spin Hamiltonian parameters are given in the text. For the simulation, Lorentzian-shaped peaks with fwhm = 800 G were assumed.

parameter of D = −4.1 cm, and, additionally, a very small rhombicity of $|E| \approx 0.04$ cm^{-1} was included to give better agreement with the experimental data. The apparent axiality is justified by the close proximity to local D_{4h} point-group symmetry by the holohedrized ligand field. This introduction of $|E|$ = 0.04 cm^{-1} has no visible influence on the INS spectra. In fact, it leads to a splitting of the |1, ±1⟩ amounting to only ~0.3 cm^{-1}, which is far below the resolution limit. It should be emphasized that the magnitude of the exchange interaction has only a very limited effect on the EPR spectra and is therefore most reliably extracted from INS.

ESI mass spectra (Figures S1−S3 in the SI) of **1** in MeCN show the base peak (m/z 547.2) corresponding to $[Mn^{III}_2(\mu\text{-}F)F_4(Me_3tacn)_2]^+$ with smaller peaks at m/z 830.3 and 1239.4 corresponding to $[(Me_3tacn)_2Mn^{III}_2F_5)\cdot Mn^{III}F_3(Me_3tacn)]^+$ and $[((Me_3tacn)_2Mn^{III}_2F_5)_2\cdot PF_6]^+$, respectively. The mass

dx.doi.org/10.1021/ic500049w | Inorg. Chem. 2014, 53, 5013−5019

spectrometric results suggest that the dinuclear complex in **1** is largely conserved in an acetonitrile solution. This is corroborated by the absence of any peaks in the range corresponding to monomeric fragments, viz., below m/z 350. Solid-state reflectance spectra and the UV−vis spectrum acquired in a MeCN solution are shown in Figure 7. The

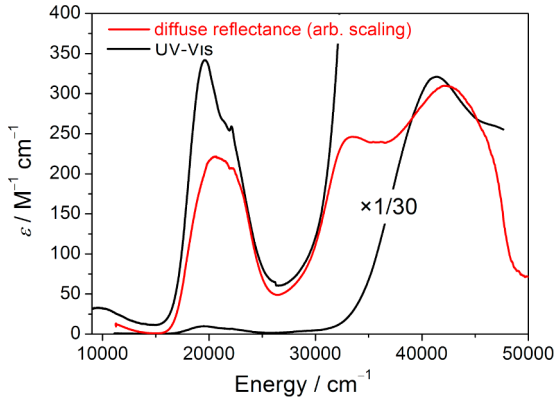

Figure 7. UV−vis absorption (MeCN solution) and diffuse reflectance spectra of **1**. The reflectance was converted to absorption by a Kubelka−Monk transformation and scaled arbitrarily.

reflectance data reveal three prominent absorption peaks at 20500 cm^{-1} (488 nm), 33500 cm^{-1} (299 nm), and 42300 cm^{-1} (236 nm). In addition, a sharp, weak feature reminiscent of a spin-forbidden transition is observed at 22200 cm^{-1} (450 nm). The solution UV−vis spectrum strongly resembles the solid-state reflectance data with three prominent peaks at 19600 cm^{-1} (510 nm, 342 M^{-1} cm^{-1}) and 41400 cm^{-1} (242 nm, ∼9600 M^{-1} cm^{-1}) and a characteristic spin-forbidden transition at 22100 cm^{-1} (453 nm). Additionally, a broad, weak band is observed at 9690 cm^{-1} (1044 nm, 32.9 M^{-1} cm^{-1}). The latter is assigned to the $^5A_{1g} \leftarrow {}^5B_{1g}$ transition. These states are labeled as irreps of the D_{4h} point group, the pertinent approximate holohedrized symmetry of the ligand field, as discussed above. This transition energy between these tetragonal split components of the octahedrally derived $^5E_g(O_h)$,[39] has for orthoaxial ligation the exact expression $E(^5A_{1g}) - E(^5B_{1g}) = 2(e_\sigma^{eq} - e_\sigma^{ax})$ independent of the internal field strength, Δ/B. Hence, a σ anisotropy of magnitude $e_\sigma^{eq} \approx e_\sigma^{ax} = 4800$ cm^{-1} can be directly inferred from the solution spectrum. The peaks around 500 nm are assigned to the only other spin-allowed d−d transitions of the high-spin d^4 configuration: $[^5B_{2g}, {}^5E_g] \leftarrow {}^5B_{1g}$. $^5B_{2g}$ and ^5E_g are the split components of octahedrally derived $^5T_{2g}$ and, consequently, to first order, $\Delta_O = [E(^5B_{2g}) + 2E(^5E_g)]/3 - [E(^5A_{1g}) + E(^5B_{1g})]/2$. Employing this expression and Gaussian deconvolution of the spectrum below 25000 cm^{-1} (Figure S7 in the SI) yields a value of $\Delta_O \approx 16100$ cm^{-1}, which is ca. 14% higher than that for $[MnF_6]^{3-}$ (14100 cm^{-1})[40] but because of JT distortion is ca. 6% lower than that for *fac*-$[CrF_3(Me_3tacn)]$.[29b]

DISCUSSION

In sharp contrast to bridging oxide, for which the properties as a mediator of magnetic exchange in molecular systems have been rigorously investigated,[41] similar studies of isoelectronic fluoride are, except for a few, recent reports by Reger and co-workers,[42] essentially nonexistent. Detailed studies of magnetic exchange have only been performed for M−F−M with M = Mn^{II},[4a,42c] Cr^{III},[43] Fe^{II},[44,42c] Co^{II},[42c] Ni^{II},[42c] and Cu^{II}.[42b,c] The strength of the exchange interaction in **1** is close to the value found for the MnF(salen) chain and other extended manganese(III) systems with linear or close-to-linear fluoride bridges.[12,13] As discussed by Pebler et al.[45] and Palacio and Morón,[12] for purely inorganic, one-dimensional systems such as the $A_2Mn^{III}F_5 \cdot xH_2O$ family, the Mn−F−Mn bridging angle varies from 121.5° to 180° for $Li_2Mn^{III}F_5$ and $Cs_2Mn^{III}F_5 \cdot H_2O$, respectively. This structural change has a concomitantly large effect on the intrachain magnetic exchange coupling constant for which J = 8.5 and 27.0 cm^{-1} for the Li^+ and Cs^+ derivatives, respectively. It was argued that the main contribution to the magnetic superexchange arises from the $Mn(d_{z^2})$−$F(p_z)$ σ overlap, which, upon bending with an angle α, decreases as $\cos^2(\alpha)$. The slightly weaker J in $Cs_2Mn^{III}F_5 \cdot H_2O$ compared to **1** can be rationalized by the longer Mn···Mn distance of 4.25 Å in the former.[46]

The Mn−Mn interaction in **1** and the extended systems are all much weaker than that found in linear or close-to-linear dinuclear manganese(III) systems bridged by oxide. This effect cannot solely be ascribed to the longer Mn−F bonds over Mn−O bonds even if one assumes a very pessimistic scaling law. Another important difference between fluoride and oxide bridging, which actually contributes to strengthening the interaction in the fluoride-bridged systems, is the orientation of the JT axis inherent to high-spin d^4. For all polynuclear manganese(III) fluoride systems, the JT axis is directed along the Mn−F−Mn linkage, whereas its coincidence with an Mn−O−Mn axis has not been observed in any complex with an unsupported oxide bridge. In order to gain more insight into the exchange interaction, BS DFT calculations were employed. The computational details are given in the Experimental Section. The calculated value of J was obtained as

$$J = \frac{E_F - E_{BS}}{\langle \hat{S}^2 \rangle_F - \langle \hat{S}^2 \rangle_{BS}} \quad (2)$$

where E_F and E_{BS} are the absolute energies of the ferromagnetically coupled and BS states, respectively, and the other symbols have their usual meaning. Using the procedure outlined in the Experimental Section and the structure metrics obtained from crystallography yields J = 41.8 cm^{-1} in reasonable agreement with the experimental value. Geometry optimization of the structure in a vacuum results in a slight overestimation of the JT distortion with a linear bridge and bond lengths of Mn−$F_{bridging}$ 2.062 Å, Mn−$F_{terminal}$ 1.806 and 1.807 Å, and Mn−N 2.136, 2.138, and 2.311 Å. The slightly longer bridging distances in the optimized structure improve the agreement between the experimental and computed values for J, which for the optimized geometry is 39.1 cm^{-1}. The computed spin-density distribution for the high-spin state (Figure 8 and Table S1 in the SI) reveals a significant difference in the spin distribution along the JT axis and perpendicular to it: along the JT axis, there is spin delocalization with significant density on the bridging fluoride and terminal nitrogen donors. Conversely, spin polarization of the equatorial fluoride and nitrogen donors results in the opposite sign of spin densities on these ligators.

With the geometry still experimentally determined but a bridging oxide substituted for the bridging fluoride, the exchange coupling constant for $[Mn^{III}_2(\mu\text{-}O)F_4(Me_3tacn)_2]$ is calculated to be J = 139.1 cm^{-1}. Geometry optimization of the latter species causes the JT axes to switch to being along one of the equatorial fluoride directions. The oxide bridge remains

dx.doi.org/10.1021/ic500049w | Inorg. Chem. 2014, 53, 5013−5019

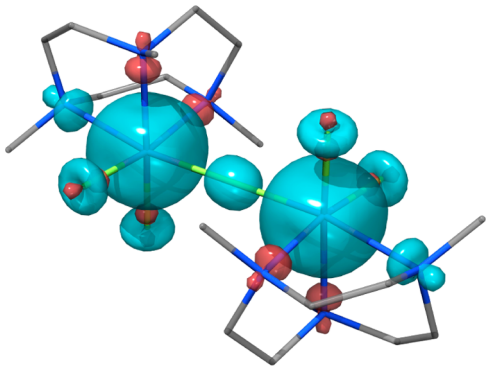

Figure 8. Spin densities in the high-spin state of the BS calculation. Isosurface values are ±0.007 $Å^{-3}$.

essentially linear (179.24°) as expected. Optimized bond lengths are Mn−$O_{bridging}$ 1.781/1.783 Å, Mn−$F_{terminal}$ 1.872/1.865 and 1.970/1.974 Å, Mn−N_{axial} 2.159/2.163 Å, and Mn−$N_{equatorial}$ 2.235/2.223 and 2.412/2.415 Å. Despite the switch of the JT axis, a larger exchange coupling constant of J = 189.3 cm^{-1} is calculated for the geometry-optimized oxide bridge structure because of the significantly shorter bond lengths in the bridge.

CONCLUSIONS

In summary, the combined use of magnetic measurements, INS, and HF-EPR allows for the precise determination of the electronic ground and low-lying excited states in a fluoride-bridged dinuclear manganese(III) complex. Magnetic exchange interactions through linearly bridging fluoride between manganese(III) are 1 order of magnitude smaller than those compared to isoelectronic oxide but comparable in magnitude to interactions via bridging cyanide ligands, which are so ubiquitous in molecule-based magnetism.[47] The determined magnitude of the interactions has initiated our interest in obtaining other antiferro- and ferrimagnetic systems incorporating fluoride bridges between manganese(III) and other transition-metal ions. The synthesis of such systems has proven feasible, and initial studies will be reported in due course.

ASSOCIATED CONTENT

Supporting Information

X-ray crystallographic data in CIF format, additional INS, HF-EPR, UV−vis, and mass spectra, and DFT results. This material is available free of charge via the Internet at http://pubs.acs.org.

AUTHOR INFORMATION

Corresponding Author

*E-mail: bendix@kiku.dk. Tel: +45 35 32 01 11. Fax: +45 35 32 02 14.

Author Contributions

All authors have given approval to the final version of the manuscript.

Notes

The authors declare no competing financial interest.

ACKNOWLEDGMENTS

K.S.P. thanks "DANSCATT—Danish Centre for Use of Synchrotron and Neutron Facilities" for financial support and the Danish Ministry of Science, Innovation and Higher Education for an EliteForsk Travel Scholarship. J.B. and H.W. acknowledge support from the Danish Research Council for Independent Research (Grant 12-125226).

REFERENCES

(1) Ako, A. M.; Hewitt, I. J.; Mereacre, V.; Clérac, R.; Wernsdorfer, W.; Anson, C. E.; Powell, A. K. *Angew. Chem., Int. Ed.* **2006**, *45*, 4926.

(2) (a) Sessoli, R.; Gatteschi, D.; Caneschi, A.; Novak, M. A. *Nature* **1993**, *365*, 141. (b) Christou, G.; Gatteschi, D.; Hendrickson, D. N.; Sessoli, R. *MRS Bull.* **2000**, *25*, 66. (c) Gatteschi, D.; Sessoli, R. *Angew. Chem., Int. Ed.* **2003**, *42*, 268. (d) Aromi, G.; Brechin, E. K. In *Single-Molecule Magnets and Related Phenomena*; Winpenny, R., Ed.; Springer-Verlag: Berlin, 2006; Vol. *122*.

(3) (a) Clérac, R.; Miyasaka, H.; Yamashita, M.; Coulon, C. *J. Am. Chem. Soc.* **2002**, *124*, 12837. (b) Coulon, C.; Miyasaka, H.; Clérac, R. In *Single-Molecule Magnets and Related Phenomena*; Winpenny, R., Ed.; Springer-Verlag: Berlin, 2006; Vol. *122*.

(4) (a) Meally, S. T.; Mason, K.; McArdle, P.; Brechin, E. K.; Ryder, A. G.; Jones, L. F. *Chem. Commun.* **2009**, 7024. (b) Dreiser, J.; Pedersen, K. S.; Piamonteze, C.; Rusponi, S.; Salman, Z.; Ali, M. E.; Schau-Magnussen, M.; Thuesen, C. A.; Piligkos, S.; Weihe, H.; Mutka, H.; Waldmann, O.; Oppeneer, P.; Bendix, J.; Nolting, F.; Brune, H. *Chem. Sci.* **2012**, *3*, 1024. (c) Birk, T.; Pedersen, K. S.; Thuesen, C. A.; Weyhermueller, T.; Schau-Magnussen, M.; Piligkos, S.; Weihe, H.; Mossin, S.; Evangelisti, M.; Bendix, J. *Inorg. Chem.* **2012**, *51*, 5435. (d) Thuesen, C. A.; Pedersen, K. S.; Schau-Magnussen, M.; Evangelisti, M.; Vibenholt, J.; Piligkos, S.; Weihe, H.; Bendix, J. *Dalton Trans.* **2012**, *41*, 11284. (e) Singh, S. K.; Pedersen, K. S.; Sigrist, M.; Thuesen, C. A.; Schau-Magnussen, M.; Mutka, H.; Piligkos, S.; Weihe, H.; Rajaraman, G.; Bendix, J. *Chem. Commun.* **2013**, *49*, 5583.

(5) Pedersen, K. S.; Sigrist, M.; Sørensen, M. A.; Barra, A.-L.; Weyhermüller, T.; Piligkos, S.; Thuesen, C. Aa.; Vinum, M. G.; Mutka, H.; Weihe, H.; Clérac, R.; Bendix, J. *Angew. Chem., Int. Ed.* **2014**, *53*, 1351.

(6) (a) van Slageren, J.; Sessoli, R.; Gatteschi, D.; Smith, A. A.; Helliwell, M.; Winpenny, R. E. P.; Cornia, A.; Barra, A.-L.; Jansen, A. G. M.; Rentschler, E.; Timco, G. A. *Chem.—Eur. J.* **2002**, *8*, 277. (b) Affronte, M.; Carretta, S.; Timco, G. A.; Winpenny, R. E. P. *Chem. Commun.* **2007**, 1789. (c) Timco, G. A.; Faust, T. B.; Tuna, F.; Winpenny, R. E. P. *Chem. Soc. Rev.* **2011**, *40*, 3067.

(7) Ochsenbein, S. T.; Tuna, F.; Rancan, M.; Davies, R. S. G.; Muryn, C. A.; Waldmann, O.; Bircher, R.; Sieber, A.; Carver, G.; Mutka, H.; Fernandez-Alonso, F.; Podlesnyak, A.; Engelhardt, L. P.; Timco, G. A.; Güdel, H. U.; Winpenny, R. E. P. *Chem.—Eur. J.* **2008**, *14*, 5144.

(8) (a) Jones, L. F.; Brechin, E. K.; Collison, D.; Harrison, A.; Teat, S. J.; Wernsdorfer, W. *Chem. Commun.* **2002**, 2974. (b) Jones, L. F.; Brechin, E. K.; Collison, D.; Raftery, J.; Teat, S. J. *Inorg. Chem.* **2003**, *42*, 6971. (c) Jones, L. F.; Rajaraman, G.; Brockman, J.; Murugesu, M.; Sanudo, E. C.; Raftery, J.; Teat, S. J.; Wernsdorfer, W.; Christou, G.; Brechin, E. K.; Collison, D. *Chem.—Eur. J.* **2004**, *10*, 5180. (d) Jones, L. F.; Raftery, J.; Teat, S. J.; Collison, D.; Brechin, E. K. *Polyhedron* **2005**, *24*, 2443.

(9) Langley, S. K.; Moubaraki, B.; Berry, K. J.; Murray, K. S. *Dalton Trans.* **2010**, *39*, 4848.

(10) Wemple, M. W.; Adams, D. M.; Folting, K.; Hendrickson, D. N.; Christou, G. *J. Am. Chem. Soc.* **1995**, *117*, 7275.

(11) (a) Stief, R.; Massa, W. *Z. Anorg. Allg. Chem.* **2006**, *632*, 797. (b) Ahmadi, A.; Stief, R.; Massa, W.; Pebler, J. *Z. Anorg. Allg. Chem.* **2001**, *627*, 869. (c) Stief, R.; Massa, W. *Z. Anorg. Allg. Chem.* **2004**, *630*, 2502. (d) Darriet, J.; Massa, W.; Pebler, J.; Stief, R. *Solid State Sci.* **2002**, *4*, 1499.

(12) Palacio, F.; Morón, M. C. *Research Frontiers in Magnetochemistry*; World Scientific: Singapore, 1993.

(13) Birk, T.; Pedersen, K. S.; Piligkos, S.; Thuesen, C. A.; Weihe, H.; Bendix, J. *Inorg. Chem.* **2011**, *50*, 5312.

(14) Wieghardt, K.; Chaudhuri, P.; Nuber, B.; Weiss, J. *Inorg. Chem.* **1982**, *21*, 3086.

(15) Molinier, M.; Massa, W. *J. Fluorine Chem.* **1992**, *57*, 139.

(16) Sheldrick, G. M. *Acta Crystallogr.* **2008**, *A64*, 112.

(17) Tregenna-Piggott, P. L. W.; Sheptyakov, D.; Keller, L.; Klokishner, S. I.; Ostrovsky, S. M.; Palii, A. V.; Reu, O. S.; Bendix, J.; Brock-Nannestad, T.; Pedersen, K.; Weihe, H.; Mutka, H. *Inorg. Chem.* **2009**, *48*, 128.
(18) Azuah, R. T.; Kneller, L. R.; Qiu, Y.; Tregenna-Piggott, P. L. W.; Brown, C. M.; Copley, J. R. D.; Dimeo, R. M. *J. Res. Natl. Inst. Stand. Technol.* **2009**, *114*, 341.
(19) Richard, D.; Ferrand, M.; Kearley, G. J. *J. Neutron Res.* **1996**, *4*, 33.
(20) Barra, A. L.; Hassan, A. K.; Janoschka, A.; Schmidt, C. L.; Schünemann, V. *Appl. Magn. Reson.* **2006**, *30*, 385.
(21) Glerup, J.; Weihe, H. *Inorg. Chem.* **1997**, *36*, 2816.
(22) Noodleman, L. *J. Chem. Phys.* **1981**, *74*, 5737.
(23) (a) Neese, F. *ORCA 2.8*, revision 2131; Institut für Physikalische und Theoretische Chemie, Universität Bonn: Bonn, Germany, 2010. (b) Neese, F. *Coord. Chem. Rev.* **2009**, *253*, 526. (c) Sinnecker, S.; Neese, F.; Lubitz, W. *J. Biol. Inorg. Chem.* **2005**, *10*, 231.
(24) (a) Yamaguchi, K.; Takahara, Y.; Fueno, T. In *Applied Quantum Chemistry*; Smith, V., Jr., Schaefer, H., III, Morokuma, K., Eds.; Springer: Amsterdam, The Netherlands, 1986. (b) Soda, T.; Kitagawa, Y.; Onishi, T.; Takano, Y.; Shigeta, Y.; Nagao, H.; Yoshioka, Y.; Yamaguchi, K. *Chem. Phys. Lett.* **2000**, *319*, 223.
(25) Schafer, A.; Horn, H.; Ahlrichs, R. *J. Chem. Phys.* **1992**, *97*, 2571.
(26) (a) D'Souze, C. A.; McBride, W. J.; Sharkey, R. M.; Todaro, L. J.; Goldenberg, D. M. *Bioconjugate Chem.* **2011**, *22*, 1793. (b) Shetty, D.; Choi, S. Y.; Jeong, J. M.; Lee, J. Y.; Hoigebazar, L.; Lee, Y.-S.; Lee, D. S.; Chung, J.-K.; Lee, M. C.; Chung, Y. K. *Chem. Commun.* **2011**, *47*, 9732.
(27) Cheng, F.; Hector, A. L.; Levason, W.; Reid, G.; Webster, M.; Zhang, W. *Chem. Commun.* **2009**, 1334.
(28) Knopp, P.; Wieghardt, K. *Z. Naturforsch. B* **1991**, *46*, 1077.
(29) (a) Bossek, U.; Haselhorst, G.; Ross, S.; Wieghardt, K.; Nuber, B. *J. Chem. Soc., Dalton Trans.* **1994**, 2041. (b) Birk, T.; Magnussen, M. J.; Piligkos, S.; Weihe, H.; Holten, A.; Bendix, J. *J. Fluorine Chem.* **2010**, *131*, 898.
(30) Pedersen, K. S.; Lorusso, G.; Morales, J.-J.; Weyhermüller, T.; Piligkos, S.; Singh, S. K.; Larsen, D.; Schau-Magnussen, M.; Rajaraman, G.; Evangelisti, M.; Bendix, J. *Angew. Chem., Int. Ed.* **2014**, DOI: 10.1002/anie.201308240.
(31) (a) Penkert, F. N.; Weyhermüller, T.; Wieghardt, K. *Chem. Commun.* **1998**, 557.
(32) Cheng, F.; Davis, M. F.; Hector, A. L.; Levason, W.; Reid, G.; Webster, M.; Zhang, W. *Eur. J. Inorg. Chem.* **2007**, 4897.
(33) Kosog, B.; La Pierre, H. S.; Heinemann, F. W.; Liddle, S. T.; Meyer, K. *J. Am. Chem. Soc.* **2012**, *134*, 5284.
(34) Bodner, A.; Jeske, P.; Weyhermüller, T.; Wieghardt, K.; Dubler, E.; Schmalle, H.; Nuber, B. *Inorg. Chem.* **1992**, *31*, 3737.
(35) Khusnutdinova, J. R.; Rath, N. P.; Mirica, L. M. *Angew. Chem., Int. Ed.* **2011**, *50*, 5532.
(36) (a) Stuiber, S.; Wu, G.; Nehrkorn, J.; Dreiser, J.; Lan, Y. H.; Novitchi, G.; Anson, C. E.; Unruh, T.; Powell, A. K.; Waldmann, O. *Chem.—Eur. J.* **2011**, *17*, 9094. (b) Basler, R.; Boskovic, C.; Chaboussant, G.; Gudel, H. U.; Murrie, M.; Ochsenbein, S. T.; Sieber, A. *ChemPhysChem* **2003**, *4*, 910. (c) Dreiser, J.; Schnegg, A.; Holldack, K.; Pedersen, K. S.; Schau-Magnussen, M.; Nehrkorn, J.; Tregenna-Piggott, P.; Mutka, H.; Weihe, H.; Bendix, J.; Waldmann, O. *Chem.—Eur. J.* **2011**, *17*, 7492. (d) Carretta, S.; Guidi, T.; Santini, P.; Amoretti, G.; Pieper, O.; Lake, B.; van Slageren, J.; El Hallak, F.; Wernsdorfer, W.; Mutka, H.; Russina, M.; Milios, C. J.; Brechin, E. K. *Polyhedron* **2009**, *28*, 1940. (e) Pedersen, K. S.; Schau-Magnussen, M.; Bendix, J.; Weihe, H.; Palii, A. V.; Klokishner, S. I.; Ostrovsky, S.; Reu, O. S.; Mutka, H.; Tregenna-Piggott, P. L. W. *Chem.—Eur. J.* **2010**, *16*, 13458. (f) Pedersen, K. S.; Sigrist, M.; Weihe, H.; Tregenna-Piggott, P. L. W.; Schau-Magnussen, M.; Dreiser, J.; Mutka, H.; Barra, A.-L.; Bendix, J. *Inorg. Chem. Commun.* **2012**, *24*, 24. (g) Dreiser, J.; Pedersen, K. S.; Schnegg, A.; Holldack, K.; Nehrkorn, J.; Sigrist, M.; Tregenna-Piggott, P.; Mutka, H.; Weihe, H.; Mironov, V. S.; Bendix, J.; Waldmann, O. *Chem.—Eur. J.* **2013**, *19*, 3693.
(37) (a) Kennedy, B. J.; Murray, K. S. *Inorg. Chem.* **1985**, *24*, 1552. (b) Mossin, S.; Weihe, H.; Barra, A.-L. *J. Am. Chem. Soc.* **2002**, *124*, 8764.
(38) (a) Mantel, C.; Hassan, A. K.; Pécaut, J.; Deronzier, A.; Collomb, M.-N.; Duboc-Toia, C. *J. Am. Chem. Soc.* **2003**, *125*, 12337. (b) Limburg, J.; Vrettos, J. S.; Crabtree, R. H.; Brudvig, G. W.; de Paula, J. C.; Hassan, A.; Barra, A.-L.; Duboc-Toia, C.; Collomb, M.-N. *Inorg. Chem.* **2001**, *40*, 1698. (c) Albela, B.; Carina, R.; Policar, C.; Poussereau, S.; Cano, J.; Guilhem, J.; Tchertanov, L.; Blondin, G.; Delroisse, M.; Girerd, J.-J. *Inorg. Chem.* **2005**, *44*, 6959.
(39) Allen, G. C.; El-Sharkawy, G. A. M.; Warren, K. D. *Inorg. Chem.* **1971**, *10*, 2538.
(40) Köhler, P.; Massa, W.; Reinen, D.; Hofmann, B.; Hoppe, R. *Z. Anorg. Allg. Chem.* **1978**, *446*, 131.
(41) (a) Weihe, H.; Güdel, H. U. *J. Am. Chem. Soc.* **1997**, *119*, 6539. (b) Weihe, H.; Güdel, H. U. *J. Am. Chem. Soc.* **1998**, *120*, 2870.
(42) (a) Reger, D. L.; Foley, E. A.; Watson, R. P.; Pellechia, P. J.; Smith, M. D.; Grandjean, F.; Long, G. J. *Inorg. Chem.* **2009**, *48*, 10658. (b) Reger, D. L.; Pascui, A. E.; Smith, M. D.; Jezierska, J.; Ozarowski, A. *Inorg. Chem.* **2012**, *51*, 7966. (c) Reger, D. L.; Pascui, A. E.; Smith, M. D.; Jezierska, J.; Ozarowski, A. *Inorg. Chem.* **2012**, *51*, 11820.
(43) (a) Sanzenbacher, R.; Bottcher, A.; Elias, H.; Huber, M.; Haase, W.; Glerup, J.; Jensen, T. B.; Neuburger, M.; Zehnder, M.; Springborg, J.; Olsen, C. E. *Inorg. Chem.* **1996**, *35*, 7493. (b) Zhu, Q.; Nelson, K. J.; Shum, W. W.; DiPasquale, A.; Rheingold, A. L.; Miller, J. S. *Inorg. Chim. Acta* **2009**, *362*, 595.
(44) Yan, Z.; Jang, H. G.; Chiou, Y.-M.; Hendrich, M. P.; Que, L., Jr. *Inorg. Chim. Acta* **1993**, *213*, 41.
(45) Pebler, J.; Massa, W.; Lass, H.; Ziegler, B. *J. Solid State Chem.* **1987**, *71*, 87.
(46) Kauěič, V.; Bukovec, P. *Acta Crystallogr., Sect. B* **1978**, *34*, 3337.
(47) (a) Weihe, H.; Güdel, H. U. *Comments Inorg. Chem.* **2000**, *22*, 75. (b) Herrera, J M.; Bachschmidt, A.; Villain, F.; Bleuzen, A.; Marvaud, V.; Wernsdorfer, W.; Verdaguer, M. *Philos. Trans. R. Soc. London, A* **2008**, *366*, 127. (c) Wang, X. Y.; Avendaño, C.; Dunbar, K. R. *Chem. Soc. Rev.* **2011**, *40*, 3213.